

Hints for the metallic phase in Rb₄C₆₀ under pressure

Estaline Amitha Francis, Christine A. Kuntscher

Angaben zur Veröffentlichung / Publication details:

Francis, Estaline Amitha, and Christine A. Kuntscher. 2014. "Hints for the metallic phase in Rb₄C₆₀ under pressure." *physica status solidi (b)* 251 (12): 2569–73. <https://doi.org/10.1002/pssb.201451165>.

Nutzungsbedingungen / Terms of use:

licgercopyright

Dieses Dokument wird unter folgenden Bedingungen zur Verfügung gestellt: / This document is made available under these conditions:

Deutsches Urheberrecht

Weitere Informationen finden Sie unter: / For more information see:

<https://www.uni-augsburg.de/de/organisation/bibliothek/publizieren-zitieren-archivieren/publiz/>



Hints for the metallic phase in Rb_4C_{60} under pressure

E. A. Francis and C. A. Kuntscher*

Experimentalphysik 2, Universität Augsburg, 86135 Augsburg, Germany

* Corresponding author: e-mail christine.kuntscher@physik.uni-augsburg.de, Phone: +49-821-598-3315, Fax: +49-821-598-3411

1 Introduction Alkali-metal fullerides are among the most investigated class of fullerene-based compounds. By doping fullerene with alkali metal, different properties can be realized depending on the charge on the fullerene. Among the family of alkali-metal fullerides, A_3C_{60} was studied extensively as it exhibits superconductivity. A_4C_{60} compounds, in contrast, are non-metallic: The additional charge in C_{60}^{4-} causes a Jahn–Teller distortion and symmetry reduction. At ambient conditions, A_4C_{60} is described as a Mott–Jahn–Teller insulator [1]. Efforts have been made to tune A_4C_{60} toward a metallic state under pressure, and indeed a metallic phase under pressure was reported by NMR [2], which triggered high-pressure studies by several other groups. A brief review of the pressure-dependent results was presented by Yao et al. [3]. In spite of the large volume of the literature, the driving mechanism of the insulator-to-metal transition is not yet understood. Several experimental techniques have contributed in this direction, and the two possible explanations for the pressure-induced insulator-to-metal transition currently discussed in the literature are (i) the closing of the charge gap based on NMR [4] and XRD [5, 6] results, and (ii) a nanoscale phase separation based on the Raman spectra under pressure, where the presence of the metallic Rb_3C_{60} phase was concluded from the Raman-active phonon modes [3, 7]. However, the phase separation scenario has not yet been verified by other experimental techniques.

In this article we present the results of an infrared reflectivity study on Rb_4C_{60} under high pressure. Infrared

spectroscopy is a powerful technique to monitor the pressure-induced changes in the electronic properties of a material [8–12]. We will discuss in detail the possible underlying mechanism of the pressure-induced insulator-to-metal transition in Rb_4C_{60} based on our findings.

2 Experiment

2.1 Synthesis and powder XRD of Rb_4C_{60} Rb_4C_{60} powder samples were synthesized by solid-state reaction [13–16], by allowing stoichiometric amount of C_{60} and Rb to react in a stainless steel capsule at 450 °C under vacuum (10^{-6} mbar) for about 25 days. Intermediate grinding was carried out to improve the homogeneity of the sample. Rb_4C_{60} was characterized by powder X-ray diffraction (XRD), and the XRD patterns were analyzed by Le Bail fitting. Accordingly, the sample was identified as phase pure Rb_4C_{60} . The XRD pattern of Rb_4C_{60} is shown in Fig. 1 together with the expected diffraction peak positions for the different possible phases Rb_4C_{60} , Rb_3C_{60} , and Rb_6C_{60} .

2.2 High-pressure infrared reflectivity measurements Reflection measurements in the infrared frequency range were carried out with a Bruker 66v/S Fourier transform infrared spectrometer. The spectrometer is coupled to an infrared microscope Bruker IR scope II with $15\times$ magnification, in order to focus the beam on the small samples in the diamond anvil cell (DAC). The high pressure up to 8 GPa was generated by a Cryo DAC Mega (Almax easyLab). The ruby

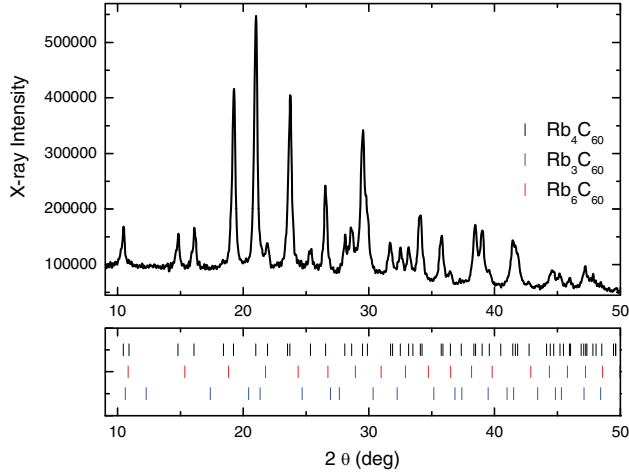


Figure 1 Powder X-ray diffraction pattern of Rb_4C_{60} together with the diffraction peak positions of possible phases Rb_4C_{60} , Rb_3C_{60} , and Rb_6C_{60} in the lower panel.

luminescence method was used for pressure determination [17]. Rb_4C_{60} pellets were made by pressing the powder sample between the pristine gasket and the diamonds of the DAC. Reflection measurements on Rb_4C_{60} pellet were performed in the far- to midinfrared (FIR–MIR) region ($100\text{--}8000\text{ cm}^{-1}$). The interface between the gasket (CuBe) and diamond was measured as the reference for normalization of the sample spectra, as illustrated in the inset of Fig. 2. Data were recorded with a resolution of 1 cm^{-1} in the frequency range $100\text{--}500\text{ cm}^{-1}$ and 2 cm^{-1} in the frequency range $500\text{--}8000\text{ cm}^{-1}$. All measurements were carried out at room temperature.

3 Results and discussion The infrared reflectivity spectra of Rb_4C_{60} as a function of pressure are depicted in Fig. 2. The frequency region around 2000 cm^{-1} is cut out from the experimental spectra, since strong diamond multiphonon absorptions cause artifacts in this spectral range. The overall reflectivity at the lowest applied pressure (0.8 GPa) is low and shows the two infrared-active T_{1u} phonon modes at 572 and 1355 cm^{-1} . The phonon at 1355 cm^{-1} shows a twofold splitting. With increasing pressure, the overall reflectivity increases and the phonon modes harden.

For a quantitative analysis, the reflectivity spectra were fitted according to the Fresnel equation for the normal-incidence reflectivity, taking into account the diamond-sample interface:

$$R_{s-d} = \left| \frac{n_{\text{dia}} - \sqrt{\epsilon_s}}{n_{\text{dia}} + \sqrt{\epsilon_s}} \right|^2, \quad (1)$$

where n_{dia} is the refractive index of the diamond which is assumed to be independent of pressure, and ϵ_s is the complex dielectric function of the sample which can be written as $\epsilon_s = \epsilon_\infty + i\sigma/(\epsilon_0\omega)$, where σ is the optical conductivity. The reflectivity spectra were fitted with the Drude–Lorentz model and the asymmetric phonons were

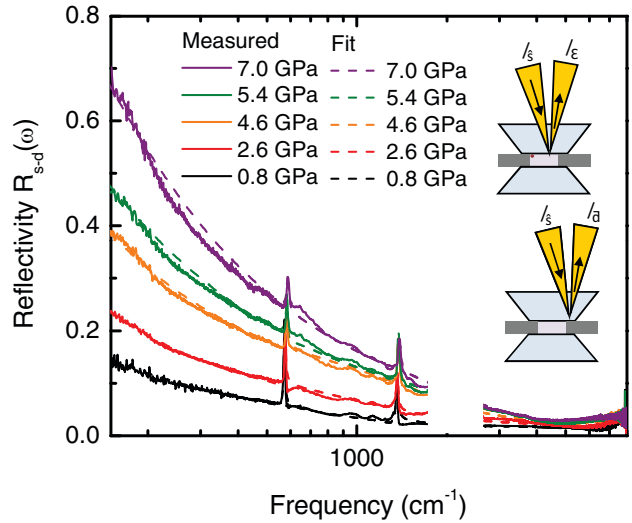


Figure 2 Infrared reflectivity spectra of Rb_4C_{60} for selected pressures together with the fitting according to the Drude–Lorentz model with a Fano approach. Inset: Reflectivity measurement configuration with the incident beam (I_i), the reflected beam from the sample (I_s), and the reference beam reflected from the gasket–diamond interface (I_r).

fitted using the Fano approach. Within the Drude–Lorentz model the complex dielectric function is described as

$$\epsilon(\omega) = \epsilon_\infty - \frac{\omega_p^2}{\omega^2 + i\omega\gamma} + \sum_i \frac{\omega_{p,i}^2}{(\omega_i^2 - \omega^2) - i\omega\gamma_i}, \quad (2)$$

where ϵ_∞ stands for the dielectric constant at high energy, ω_p the plasma frequency, the second term is the Drude component, and the last term is the Lorentz component.

According to the Fano theory [18] the interaction of one or more discrete levels with a continuum of states would result in asymmetric optical absorption peaks. After subtraction of the continuous electronic background the Fano profile is described by

$$\sigma(\omega) = \sum_j i\sigma_{oj} \frac{(q_j + i)^2}{i + x(\omega)}, \quad (3)$$

with $x(\omega) = (\omega_{0j}^2 - \omega^2)/\gamma_j\omega$, where ω_{0j} is the resonance frequency, ω_j is the damping and $\sigma_{oj} = \omega_{pj}/\gamma_j q_j^2$ with ω_{pj} as the oscillator strength, and q_j is the dimensionless asymmetry factor of the j th absorption. The fit value of the Fano parameter q describes the asymmetry of the peak. For the Fano parameter $|q| \rightarrow \infty$, a Lorentzian oscillator line shape is recovered. Furthermore, depending on the value of q , the absorption can be in resonance with phonon domination when $|q| \gg 1$, dispersive when the contribution of the phonon and electronic background are comparable ($|q| \sim 1$), or antiresonance line shape when $|q| \ll 1$ representing the domination of the electronic background.

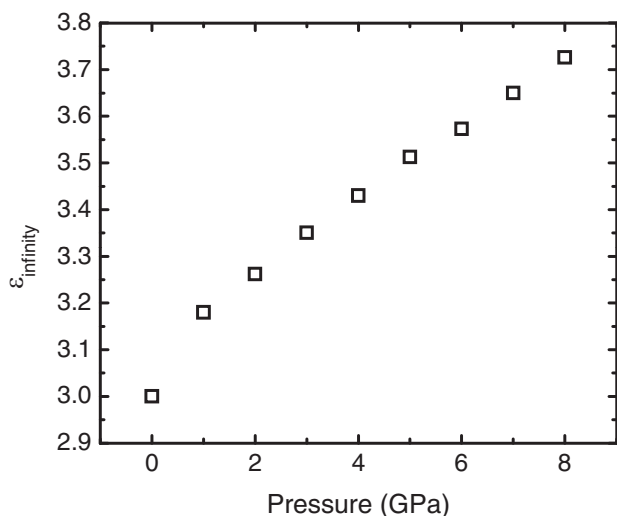


Figure 3 Calculated high-frequency permittivity ε_{∞} as a function of pressure.

To obtain a good fit of the reflectivity spectra, the value of ε_{∞} as a function of pressure was determined by using the Clausius–Mossotti equation given by [19]

$$\frac{\varepsilon_{\infty}(P) - 1}{\varepsilon_{\infty}(P) + 2} = \frac{\alpha}{3\varepsilon_0 V(P)}. \quad (4)$$

Hereby, α is the electronic polarizability of the unit cell, which is obtained from the lowest-pressure data by taking into account the corresponding unit cell volume. The pressure-dependent XRD measurements by Huq and Stephens [6] and Sabouri et al. [5] give the unit cell volume change $V(P)$ in the pressure range which is of interest here. By assuming that α is pressure independent, the high-frequency dielectric permittivity was obtained and is shown with increasing pressure in Fig. 3. With the so-obtained values of ε_{∞} , the reflectivity spectra in the FIR–MIR region were fitted with the above-described models, and a few selected spectra with the corresponding fitting curves are shown in Fig. 2. The data in the region between 1700 and 2600 cm^{-1} are not used for the analysis because of the artifacts caused by the multi-phonon absorption in the diamonds of the DAC. The two infrared-active phonons $T_{1u}(2)$ and $T_{1u}(4)$ are indeed better described by a Fano resonance profile than by the usual harmonic Lorentz oscillator, as illustrated in Fig. 4. The real part of optical conductivity $\sigma_1(\omega)$, as obtained from the fitting of the reflectivity spectra, is shown in Fig. 5 for selected pressures.

3.1 Infrared spectra of Rb_4C_{60} at lowest pressure

At lowest pressure (0.8 GPa) the real part of the optical conductivity of Rb_4C_{60} shows a small, but finite value at low frequencies as seen in Fig. 5, owing to a small Drude contribution. This low value of the low-frequency optical conductivity indicates a bad-metal behavior of Rb_4C_{60} , which is in agreement with the literature data [4]. Besides the two T_{1u} phonon

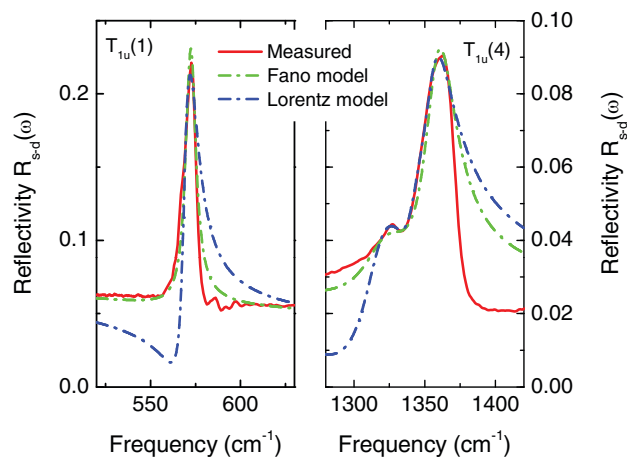


Figure 4 Reflectivity spectra of Rb_4C_{60} at 0.8 GPa in the phonon mode region together with the fits according to the Lorentz and the Fano model.

modes, a MIR band is observed at around 7000 cm^{-1} , which corresponds to the LUMO \rightarrow LUMO+1 transitions [20, 21].

The infrared phonons of Rb_4C_{60} at the lowest pressure are well described by the Fano resonance model. The down shift of the $T_{1u}(4)$ phonon mode as compared to the neutral fullerene can be attributed to the charge transfer [13]. The $T_{1u}(2)$ phonon is a singlet, while the $T_{1u}(4)$ phonon is analyzed as a doublet. According to group theory, a D_{2h} symmetry of the molecule would give rise to a triplet splitting of the $T_{1u}(4)$ phonon [13]. Based on our data we do not exclude the possibility of a threefold splitting because of the broad second branch of the $T_{1u}(4)$ mode. The Fano parameter q has a positive value for both phonons, indicating that these

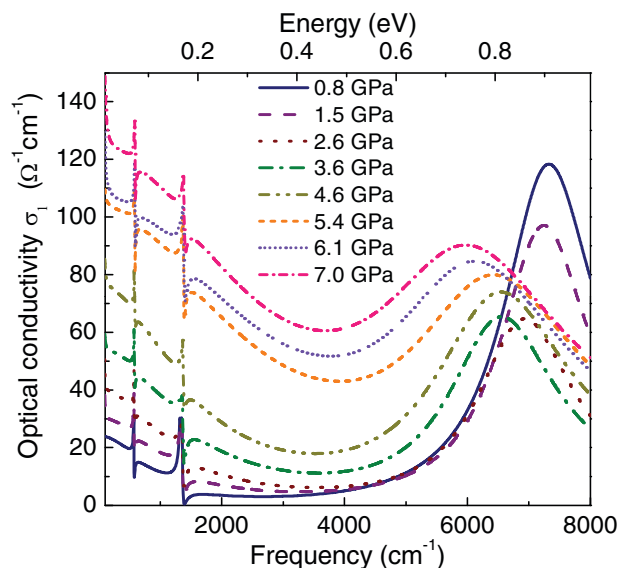


Figure 5 Real part of optical conductivity $\sigma_1(\omega)$ of Rb_4C_{60} for selected pressures, as obtained from the Drude–Lorentz fitting of the reflectivity spectra.

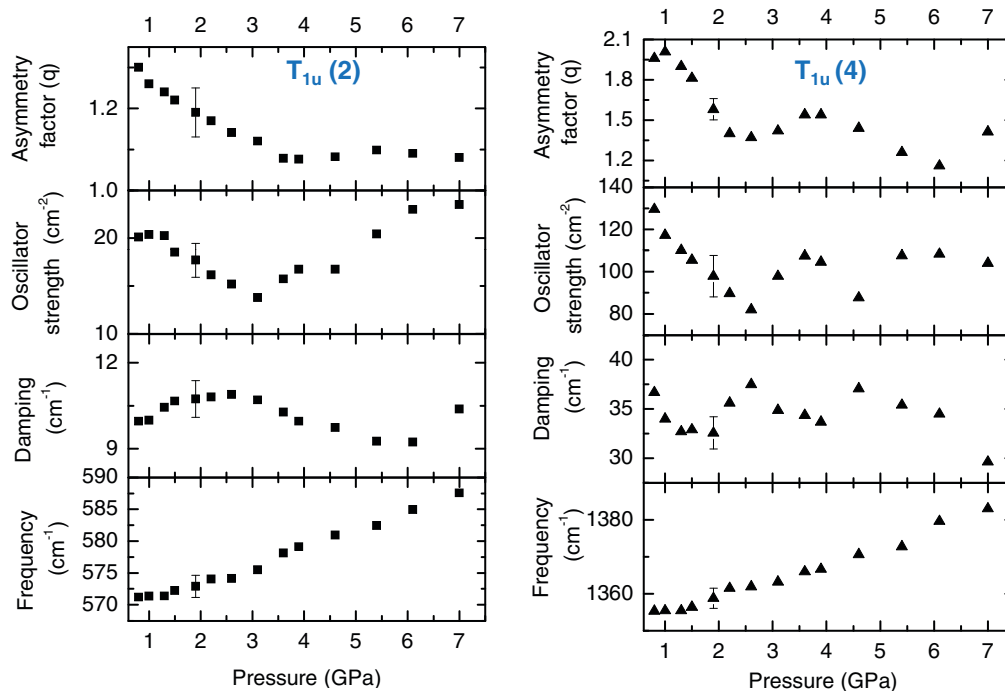


Figure 6 Pressure-dependence of the four parameters of the Fano resonance model applied for fitting the T_{1u} phonon modes.

vibrational modes are coupled with an electronic background at lower frequency, most probably the Drude term.

3.2 Pressure-dependent infrared spectra of Rb_4C_{60} The low-frequency optical conductivity of Rb_4C_{60} increases with increasing pressure (see Fig. 5), indicating an improved metallic behavior. However, the value of the low-frequency optical conductivity remains low up to the highest applied pressure, and hence the bad metal character Rb_4C_{60} is retained in the whole measured pressure range. The pressure dependence of the phonon parameters, as obtained from the fitting with the Fano resonance model, is shown in Fig. 6. Both phonon modes harden monotonically under pressure. The other fitting parameters do not show a clear pressure dependence, except the asymmetry factor q , which tends to lower values with increasing pressure. The decreasing value suggests an increasing coupling between the phonons and the electronic states. Furthermore, the redshift of the MIR electronic transitions in the fulleride ions indicates a pressure-induced broadening of the bands at a molecular level.

Yao et al. proposed that the metallic state under pressure is due to the phase separation of Rb_4C_{60} into Rb_3C_{60} and Rb_6C_{60} [3, 7]. Based on the results of our infrared measurements it is possible to comment on this phase separation scenario. The Rb_6C_{60} phase is expected to be easily detectable in the infrared spectra because of its four infrared-active phonons [22]. Therefore, if additional phonons due to Rb_6C_{60} are observed under pressure, it would indirectly confirm the appearance of the Rb_3C_{60} phase, and hence could

explain the metallic character of the sample in terms of a phase-separation scenario. In our reflectivity spectra no new phonons were observed in the whole measured pressure range. Thus, we exclude the appearance of the Rb_6C_{60} phase under pressure based on our data, which in turn makes the phase separation scenario unlikely. Therefore, the metallic character of Rb_4C_{60} under pressure could be explained by the closing of the charge gap with increasing pressure. However, a nanoscale phase separation would be below the diffraction limit of the infrared measurements [23, 24] and we would not be able to detect it.

4 Conclusions High-pressure infrared reflectivity measurements were carried out on the alkali-metal fulleride Rb_4C_{60} . The real part of optical conductivity at the lowest pressure (0.8 GPa) has a small, but finite Drude term indicating a bad metal character. With increasing pressure the Drude term increases, but the finite value of the low-frequency optical conductivity remains low, i.e., the bad metal character is retained up to 7 GPa. From the phonon excitations in the optical spectra the appearance of other alkali fulleride phases, like Rb_3C_{60} or Rb_6C_{60} , can be excluded. Thus the occurrence of a phase separation as the driving mechanism of the pressure-induced insulator-to-metal transition in Rb_4C_{60} seems to be unlikely. The observed metallic state under pressure is rather due to the closing of the charge gap.

Acknowledgements We gratefully acknowledge D. Viewig, Experimentalphysik V, Universität Augsburg, for

the XRD measurements on several alkali fulleride samples. We acknowledge financial support by the DFG (KU 1432/3-2).

References

- [1] M. Capone, M. Fabrizio, P. Giannozzi, and E. Tosatti, *Phys. Rev. B* **62**, 7619 (2000).
- [2] G. Zimmer, M. Elme, M. Mehring, and F. Rachdi, *Phys. Rev. B* **52**, 13300 (1995).
- [3] M. G. Yao, B. Sundqvist, and T. Wågberg, *Phys. Rev. B* **79**, 081403 (2009).
- [4] R. Kerkoud, P. Auban-Senzier, D. Jerome, S. Brazovskii, N. Kirova, I. Luk'yanchuk, F. Rachdi, and C. Goze, *Synth. Met.* **77**, 205 (1996).
- [5] A. Sabouri-Dodaran, M. Marangolo, C. Bellin, F. Mauri, G. Fiquet, G. Loupiau, M. Mezouar, W. Crichton, C. Herold, F. Rachdi, and S. Rabii, *Phys. Rev. B* **70**, 174114 (2004).
- [6] A. Huq and P. W. Stephens, *Phys. Rev. B* **74**, 075424 (2006).
- [7] M. Yao, T. Wågberg, A. Iwasiewicz-Wabnig, T. L. Makarova, and B. Sundqvist, *J. Phys. Conf. Ser.* **215**, 012020 (2010).
- [8] A. Pashkin, M. Dressel, and C. A. Kuntscher, *Phys. Rev. B* **74**, 165118 (2006).
- [9] C. A. Kuntscher, S. Frank, A. Pashkin, M. Hoinkis, M. Klemm, M. Sing, S. Horn, and R. Claessen, *Phys. Rev. B* **74**, 184402 (2006).
- [10] C. A. Kuntscher, S. Frank, A. Pashkin, H. Hoffmann, A. Schönleber, S. van Smaalen, M. Hanfland, S. Glawion, M. Klemm, M. Sing, S. Horn, and R. Claessen, *Phys. Rev. B* **76**, 241101(R) (2007).
- [11] C. A. Kuntscher, A. Pashkin, H. Hoffmann, S. Frank, M. Klemm, S. Horn, A. Schönleber, S. van Smaalen, M. Hanfland, S. Glawion, M. Sing, and R. Claessen, *Phys. Rev. B* **78**, 035106 (2008).
- [12] J. Kunes, L. Baldassarre, B. Schächner, K. Rabia, C. A. Kuntscher, Dm. M. Korotin, V. I. Anisimov, J. A. McLeod, E. Z. Kurmaev, and A. Moewes, *Phys. Rev. B* **81**, 035122 (2010).
- [13] G. Klupp, K. Kamarás, N. M. Nemes, C. M. Brown, and J. Leao, *Phys. Rev. B* **73**, 085415 (2006).
- [14] R. Fleming, M. Rosseinsky, A. Ramirez, D. Murphy, J. Tully, R. Haddon, T. Siegrist, R. Tycko, S. Glarum, P. Marsh, G. Dabbagh, S. M. Zahurak, A. V. Makhija, and C. Hampton, *Nature* **352**, 701 (1991).
- [15] C. A. Kuntscher, G. M. Bendele, and P. W. Stephens, *Phys. Rev. B* **55**, R3366 (1997).
- [16] D. Poirier, D. Owens, and J. Weaver, *Phys. Rev. B* **51**, 1830 (1995).
- [17] H. K. Mao, J. Xu, and P. M. Bell, *J. Geophys. Res.* **91**, 4673 (1986).
- [18] U. Fano, *Phys. Rev.* **124**, 1866 (1961).
- [19] R. Haumont, P. Bouvier, A. Pashkin, K. Rabia, S. Frank, B. Dkhil, W. A. Crichton, C. A. Kuntscher, and J. Kreisel, *Phys. Rev. B* **79**, 184110 (2009).
- [20] D. R. Lawson, D. L. Feldheim, C. A. Foss, P. K. Dorhout, C. M. Elliott, C. R. Martin, and B. Parkinson, *J. Electrochem. Soc.* **139**, 7 (1992).
- [21] W. H. Green, S. M. Gorun, G. Fitzgerald, P. W. Fowler, A. Ceulemans, and B. C. Titeca, *J. Phys. Chem.* **100**, 14892 (1996).
- [22] T. Pichler, R. Winkler, and H. Kuzmany, *Phys. Rev. B* **49**, 15879 (1994).
- [23] E. Betzig, P. L. Finn, and J. S. Weiner, *Appl. Phys. Lett.* **60**, 2484 (1992).
- [24] D. W. Pohl, W. Denk, and M. Lanz, *Appl. Phys. Lett.* **44**, 651 (1984).